Dalton Transactions

ROYAL SOCIETY OF CHEMISTRY

PAPER

View Article Online
View Journal | View Issue

Cite this: *Dalton Trans.*, 2023, **52**, 8391

Cytotoxicity of osmium(II) and cycloosmated half-sandwich complexes from 1-pyrenyl-containing phosphane ligands†

Dana Josa, [a,b] David Aguilà,[a,b] Pere Fontova,[c] Vanessa Soto-Cerrato, [d,e] Piedad Herrera-Ramírez,[a] Laia Rafols, [a] Arnald Grabulosa *[a,b] and Patrick Gamez *[a,b,f]

Five metal–arene complexes of formula [$MX_2(\eta^6$-*p*-cymene)(diR(1-pyrenyl)phosphane)] (M = Os or Ru, X = Cl or I, R = isopropyl or phenyl) and symbolized as $\mathbf{M^R_{X2}}$ were synthesized and fully characterized, namely $\mathbf{Os^{iPr}_{Cl2}}$, $\mathbf{Os^{iPr}_{I2}}$, $\mathbf{Os^{Ph}_{Cl2}}$, $\mathbf{Os^{Ph}_{I2}}$ and $\mathbf{Ru^{Ph}_{I2}}$. Furthermore, nine cyclometalated half-sandwich complexes of formula [MX-(η^6-*p*-cymene)(k^2C-diR(1-pyrenyl)phosphane)] (M = Os or Ru, X = Cl or I, R = isopropyl or phenyl) or [M(η^6-*p*-cymene)(*k*S-dmso)(k^2C-diR(1-pyrenyl)phosphane)]PF_6 (M = Os or Ru, R = isopropyl or phenyl) and symbolized as $\mathbf{c\text{-}M^R_X}$ were prepared; hence, $\mathbf{c\text{-}Os^{iPr}_{Cl}}$, $\mathbf{c\text{-}Os^{iPr}_{I}}$, $\mathbf{c\text{-}Os^{iPr}_{dmso}}$, $\mathbf{c\text{-}Os^{Ph}_{Cl}}$, $\mathbf{c\text{-}Os^{Ph}_{I}}$, $\mathbf{c\text{-}Os^{Ph}_{dmso}}$, $\mathbf{c\text{-}Ru^{Ph}_{Cl}}$, $\mathbf{c\text{-}Ru^{Ph}_{I}}$ and $\mathbf{c\text{-}Ru^{Ph}_{dmso}}$ were obtained and fully characterized. The crystal structures of ten out of the fourteen complexes were solved. All complexes exhibit notable cytotoxic properties against A549 (Lung Adenocarcinoma) human cells, with IC_{50} values ranging from 48 to 1.42 μM. In addition, complex $\mathbf{c\text{-}Os^{iPr}_{dmso}}$ shows remarkable toxic behaviours agains other cell lines, namely MCF7 (breast carcinoma), MCF10A (non-tumorigenic epithelial breast) and MDA-MB-435 (melanoma) human cells, as illustrated by IC_{50} values of 4.36, 4.71 and 2.32 μM, respectively. Finally, it has been found that $\mathbf{Os^{iPr}_{I2}}$ affects the cell cycle of A549 cells, impeding their replication (*i.e.*, the cell cycle is blocked), whereas $\mathbf{Os^{Ph}_{I2}}$ (namely with phenyl groups instead of isopropyl ones) does not induce this effect.

Received 10th March 2023,
Accepted 26th May 2023

DOI: 10.1039/d3dt00743j

rsc.li/dalton

Introduction

The search for new anticancer agents with increased efficiency and less unpleasant side effects is a topical area of research, for instance in bioinorganic chemistry.[1–4] Metal-based chemotherapeutic drugs have gained increasing interest after the discovery of cisplatin, *viz. cis*-diamminedichloridoplatinum(II), in 1965 by Rosenberg.[5,6] In the context of the development of alternative systems, some ruthenium-containing compounds were found to be promising anticancer drug candidates,[7–9] including ruthenium(II)–arene complexes,[4,10,11] like [RuCl(η^6-fluorene)(ethylenediamine)]PF_6, [RuCl(η^6-5,6-dihydrophenanthrene)(ethylenediamine)]PF_6 or [$RuCl_2$(η^6-*p*-cymene)(pta)] (*i.e.*, RAPTA-C with pta = 1,3,5-triaza-7-phosphaadamantane).[12,13] Many osmium(II)–arene analogues of such organoruthenium(II) compounds have subsequently been reported,[14,15] and the effect of the metal exchange on the cytotoxic properties appears not to be predictable.[16–18] In some cases, the Os(II) complexes are more active than their Ru(II) counterparts,[19–21] whereas no differences or lower activities for the Os(II) compounds were observed with other systems.[22–24]

A few years ago, we started to develop a family of ruthenium(II)–arene complexes of general formula [RuX_2(η^6-arene)(P(1-pyrenyl)R^2R^3)] (Scheme 1a, M = Ru), which displayed interesting cytotoxic properties, with IC_{50} values down to 0.4 μM.[25] We also found that such Ru(II) compounds containing a phosphane ligand with a 1-pyrenyl group could undergo cyclometalation in the presence of a base, generating complexes of formula [RuX(η^6-arene)(k^2C-(P(1-pyrenyl)R^2R^3))] or [Ru(η^6-arene)(k^2C-(P(1-pyrenyl)R^2R^3))(dmso)]PF_6 (Scheme 1b, M =

[a]*Departament de Química Inorgànica i Orgànica, Facultat de Química, Secció de Química Inorgànica, Universitat de Barcelona, Martí i Franquès, 1-11, 08028 Barcelona, Spain. E-mail: arnald.grabulosa@qi.ub.es, patrick.gamez@qi.ub.es*
[b]*Institute of Nanoscience and Nanotechnology (IN²UB), Universitat de Barcelona, 08028 Barcelona, Spain*
[c]*Department of Chemistry, Universidad de Burgos, 09001 Burgos, Spain*
[d]*Department of Pathology and Experimental Therapeutics, Faculty of Medicine and Health Sciences, Universitat de Barcelona, Campus Bellvitge, Feixa LLarga s/n, 08907 L'Hospitalet de Llobregat, Spain*
[e]*Oncobell Program, Institut d'Investigació Biomèdica de Bellvitge (IDIBELL), 08908 L'Hospitalet de Llobregat, Spain*
[f]*Catalan Institution for Research and Advanced Studies, Passeig Lluís Companys 23, 08010 Barcelona, Spain*

†Electronic supplementary information (ESI) available. CCDC 2237617–2237626. For ESI and crystallographic data in CIF or other electronic format see DOI: https://doi.org/10.1039/d3dt00743j

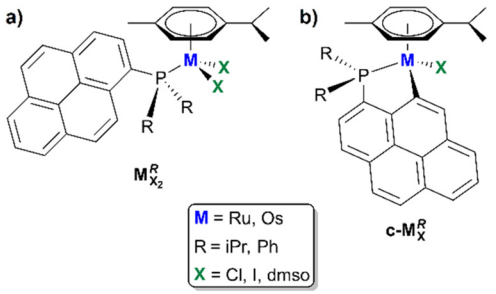

Scheme 1 Representations of (a) the piano-stool complexes based on a dialkyl/aryl(1-pyrenyl)phosphane ligand and (b) the cyclometalated (phosphane)metal complexes described earlier[25–27] and in the present study.

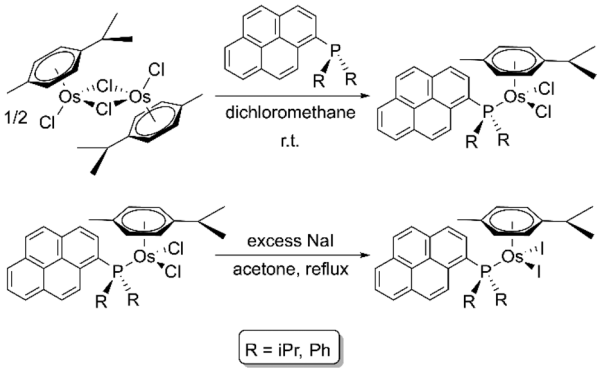

Fig. 1 Synthetic procedures used to prepare the non-cyclometalated chlorido (top) and iodido (bottom) osmium(II) complexes.

Ru).[26] Such cyclometalated piano-stool complexes displayed better cytotoxic activities than their non-cyclometalated analogues.[27]

In the present study, we investigated the effect of the replacement of Ru(II) with Os(II) on the cytotoxic behaviour in this family of organometallic compounds. It is indeed generally found that substitutions reactions (*e.g.* aquation) of Os(II) complexes are slower than for the analogous Ru(II) complexes.[28–31] Hence, we prepared a series of $[OsX_2(\eta^6\text{-}p\text{-cymene})(P(1\text{-pyrenyl})R^2R^3)]$ complexes (Scheme 1a, M = Os) with diisopropyl-(1-pyrenyl)phosphane or diphenyl-(1-pyrenyl) phosphane as monodentate phosphane ligand ($R^2 = R^3$ = isopropyl or phenyl) and chloride or iodide as anions (X = Cl or I). Moreover, the corresponding cyclometalated complexes, namely $[OsX(\eta^6\text{-}p\text{-cymene})(k^2C\text{-}(P(1\text{-pyrenyl})R^2R^3))]$ and $[Os(\eta^6\text{-}p\text{-cymene})(k^2C\text{-}(P(1\text{-pyrenyl})R^2R^3))(dmso)]PF_6$, were synthesized as well (Scheme 1b, M = Os). In addition, the cyclometalated ruthenium(II) complexes $[RuX(\eta^6\text{-}p\text{-cymene})(k^2C\text{-diphenyl(1-pyrenyl)phosphane})]$ (X = Cl or I) and $[Ru(\eta^6\text{-}p\text{-cymene})(k^2C\text{-diphenyl(1-pyrenyl)phosphane})(dmso)]PF_6$ (Scheme 1b, M = Ru; $R^2 = R^3$ = phenyl) were prepared to complete the series of Ru(II) compounds described previously and for comparison purposes with the newly reported Os(II) complexes. The biological properties of the new compounds were subsequently investigated and compared with those of the previously described complexes.

Results and discussion

Synthesis of the organometallic complexes

The ligands diisopropyl(1-pyrenyl)phosphane (**PPyriPr$_2$**)[27] and diphenyl(1-pyrenyl)phosphane (**PPyrPh$_2$**)[25] were prepared as described earlier. The non-cyclometalated osmium(II) complexes were synthesized as illustrated in Fig. 1.

The chlorido complexes were typically obtained by reaction of the osmium dimeric precursor $[OsCl(\mu\text{-}Cl)(\eta^6\text{-}p\text{-cymene})]_2$ with the phosphane ligand in dichloromethane at room temperature (Fig. 1, top). The corresponding iodido complexes were prepared through halide exchange, in the presence of an excess of sodium iodide in technical acetone under reflux (Fig. 1, bottom).

The chlorido cyclometalated complexes were synthesized by reaction of the dimeric precursors (ruthenium or osmium) with the phosphane ligand in the presence of 3 equivalents of base, namely sodium acetate, in methanol at room temperature (Fig. 2 top). The iodido cyclometalated complexes were obtained through halide exchange, using 24 equivalents of sodium iodide in acetone under reflux (Fig. 2, middle). Finally, the cationic cyclometalated complexes containing an S-coordinated DMSO molecule were prepared by reaction of the corresponding chlorido cyclometalated complexes with 10 equivalents of DMSO and 1.1 equivalent of thallium hexafluorophosphate in dichloromethane at room temperature (Fig. 2, bottom).

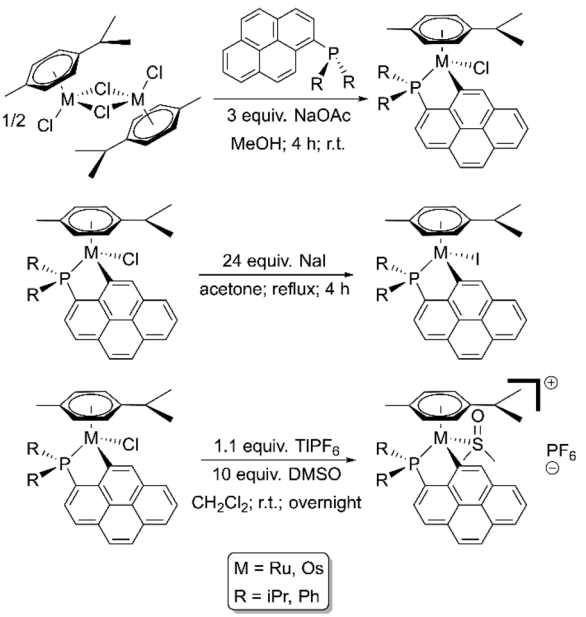

Fig. 2 Synthetic procedures to prepare the chlorido cyclometalated complexes (top), iodido cyclometalated complexes (middle) and cationic cyclometalated complexes with an S-coordinated DMSO molecule (bottom).

10 osmium(II) and 4 ruthenium(II) complexes were obtained applying these synthetic procedures, which are listed in Table 1. It can be pointed out that **c-Os$^{Ph}_{I}$** could not be prepared from **c-Os$^{Ph}_{Cl}$** through halide exchange (Fig. 2, middle). Instead, **c-Os$^{Ph}_{I}$** was synthesized by reaction of the dimeric precursor [OsI(μ-I)(η^6-*p*-cymene)]$_2$ with diphenyl(1-pyrenyl)phosphane in the presence of NaOAc.

Crystal structures

Single crystals could be obtained for 10 out of the 14 complexes prepared. Hence, crystal data and structure refinement parameters are listed in Table S1† for complexes **Os$^{iPr}_{Cl2}$**, **Os$^{iPr}_{I2}$**, **c-Os$^{iPr}_{Cl}$** and **c-Os$^{iPr}_{I}$**, Table S2† for **Os$^{Ph}_{Cl2}$**, **Os$^{Ph}_{I2}$** and **c-Os$^{Ph}_{Cl}$**, and Table S3† for **c-Ru$^{Ph}_{Cl}$**, **c-Ru$^{Ph}_{I}$** and **c-Ru$^{Ph}_{dmso}$**. Selected bond lengths and angles are given in Tables S4–S6.† Since the solid-state structures of the non-cyclometalated and cyclometalated complexes are comparatively analogous, solely the structures of **Os$^{iPr}_{Cl2}$** and **c-Os$^{iPr}_{Cl}$** are subsequently described.

A representation of the crystal structure of **Os$^{iPr}_{Cl2}$** is shown in Fig. 3. **Os$^{iPr}_{Cl2}$** crystallises in the triclinic space group $P\bar{1}$ (Table S1†).

Os$^{iPr}_{Cl2}$ exhibits the characteristic "three-legged piano-stool" geometry for this type of organoosmium(II) complexes. The Os–Cl bond lengths are 2.41 Å and the Os–P bond distance is 2.39 Å (Table S4†). The distance between the *p*-cymene ring centroid and the osmium atom is 1.70 Å. These values are comparable with those previously reported for analogous compounds.[27,32–34] The coordination angles vary from 85 to 128° (Table S4†), which is within the expected range for such molecules.[35,36] The solid-state structures of non-cyclometalated complexes **Os$^{iPr}_{I2}$**, **Os$^{Ph}_{Cl2}$** and **Os$^{Ph}_{I2}$** are depicted in Fig. S1, S3 and S4,† respectively. These compounds display coordination features that are analogous to those of **Os$^{iPr}_{Cl2}$** (see Tables S4 and S5†). It can be noted that, as expected, the Os–I bond distances are longer than the Os–Cl ones, by about 0.3 Å (Tables S4 and S5†).[27]

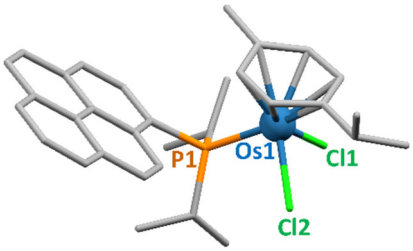

Fig. 3 Representation of the crystal structure of **Os$^{iPr}_{Cl2}$**. The atoms bonded to the metal centre are labelled. Hydrogen atoms are omitted for clarity.

The cyclometalated complex **c-Os$^{iPr}_{Cl}$** crystallises in the monoclinic space group $P2_1/c$ (Table S1†). A representation of its crystal structure is shown in Fig. 4.

The pseudo-octahedral geometry of the Os centre of **c-Os$^{iPr}_{Cl}$** is strongly distorted, as the result of the cyclometalation involving the 1-pyrenyl ring. The Os–Cl, Os–P, Os–C and Os–centroid distances are 2.43, 2.32, 2.11 and 1.73 Å, respectively (Table S4†). These bond lengths are similar to those of analogous Ru(II) complexes.[27,37,38] The coordination angles span from 81 to 133° (Table S4†), which is in the range of related Ru(II) complexes.[26] It can be stressed here that this type of cycloosmated complexes (from a monophosphane ligand) was not found in the Cambridge Structural Database (CSD, accessed in November 2022). To the best of our knowledge, compounds **c-Os$^{iPr}_{Cl}$**, **c-Os$^{iPr}_{I}$** and **c-Os$^{Ph}_{Cl}$** therefore represent the first examples of such cyclometalated osmium(II) complexes that have been characterized by X-ray diffraction.

The cycloosmated compounds **c-Os$^{iPr}_{I}$** and **c-Os$^{Ph}_{Cl}$** exhibit structural features comparable to those of **c-Os$^{iPr}_{Cl}$** (Tables S4 and S5†).

Cell viability studies

The ability of the Os(II) compounds **Os$^{iPr}_{Cl2}$**, **Os$^{iPr}_{I2}$**, **c-Os$^{iPr}_{Cl}$**, **c-Os$^{iPr}_{I}$** and **c-Os$^{iPr}_{dmso}$** was assessed against human lung adenocarcinoma (A549) cells. Half-maximum inhibitory concen-

Table 1 List of the 14 new complexes prepared in the present study with their corresponding labelling (see Scheme 1 for the representation of their corresponding structure). The complexes for which an X-ray crystal structure could be obtained are mentioned through the corresponding figure

Complex	M	R	X	X-ray structure
Os$^{iPr}_{Cl2}$	Os	Isopropyl	Cl	Fig. 3
Os$^{iPr}_{I2}$	Os	Isopropyl	I	Fig. S1†
c-Os$^{iPr}_{Cl}$	Os	Isopropyl	Cl	Fig. 4
c-Os$^{iPr}_{I}$	Os	Isopropyl	I	Fig. S2†
c-Os$^{iPr}_{dmso}$	Os	Isopropyl	dmso	n.d.[a]
Os$^{Ph}_{Cl2}$	Os	Phenyl	Cl	Fig. S3†
Os$^{Ph}_{I2}$	Os	Phenyl	I	Fig. S4†
c-Os$^{Ph}_{Cl}$	Os	Phenyl	Cl	Fig. S5†
c-Os$^{Ph}_{I}$	Os	Phenyl	I	n.d.[a]
c-Os$^{Ph}_{dmso}$	Os	Phenyl	dmso	n.d.[a]
Ru$^{Ph}_{I2}$	Ru	Phenyl	I	n.d.[a]
c-Ru$^{Ph}_{Cl}$	Ru	Phenyl	Cl	Fig. S6†
c-Ru$^{Ph}_{I}$	Ru	Phenyl	I	Fig. S7†
c-Ru$^{Ph}_{dmso}$	Ru	Phenyl	dmso	Fig. S8†

[a] n.d. = not determined (as single crystals could not be obtained).

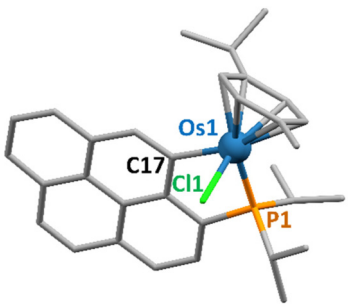

Fig. 4 Representation of the crystal structure of **c-Os$^{iPr}_{Cl}$**. The atoms bonded to the metal centre are labelled. Hydrogen atoms are omitted for clarity.

trations (IC_{50}) were determined for all compounds after an incubation time of 24 h and using freshly prepared stock solutions of the complexes in DMSO. The IC_{50} values obtained are listed in Table 2. These values were compared with those reported earlier for the corresponding Ru(II) compounds, namely compounds $\mathbf{Ru^{iPr}_{Cl2}}$, $\mathbf{Ru^{iPr}_{I2}}$, $\mathbf{c\text{-}Ru^{iPr}_{Cl}}$, $\mathbf{c\text{-}Ru^{iPr}_{I}}$ and $\mathbf{c\text{-}Ru^{iPr}_{dmso}}$.

After 24 h incubation, the non-cyclometalated osmium complexes $\mathbf{Os^{iPr}_{Cl2}}$ and $\mathbf{Os^{iPr}_{I2}}$ appear to be more active than their ruthenium counterparts (Table 2). It can be pointed out here that for the Ru(II) compounds an increase of cytotoxicity was observed with ageing solutions of $\mathbf{Ru^{iPr}_{I2}}$; for instance, a 7-day-old DMSO solution of $\mathbf{Ru^{iPr}_{I2}}$ gave an IC_{50} value of 9.5 μM (*vs.* 48 μM at day 0).[27] Cell viability assays have been performed for both $\mathbf{Os^{iPr}_{Cl2}}$ and $\mathbf{Os^{iPr}_{I2}}$ using 7-day-old DMSO solutions but no cytotoxicity differences were observed compared to the freshly prepared solutions (data not shown). Finally, it can be emphasized that the low IC_{50} value obtained for $\mathbf{Os^{iPr}_{I2}}$ appears to result from its perturbing effect on the cell cycle, since no significant cell death was observed, unlike with the other compounds. Therefore, cell cycle studies have been carried out with this complex, which are discussed below.

Regarding the cyclometalated complexes, in all cases, lower IC_{50} values are observed for the Ru(II) complexes, which are 2.5-to-3.2 times more active than the Os(II) ones.

In a previous study with analogous Ru(II) complexes, it was observed that the complex $\mathbf{c\text{-}Ru^{iPr}_{dmso}}$ was the most efficient compound and it appears to be the case as well for the Os(II) complexes (see Table 2). Thus, cell viability studies were subsequently performed with $\mathbf{c\text{-}Os^{iPr}_{dmso}}$ against various cancer and healthy cell lines, namely breast adenocarcinoma (MCF7), non-tumorigenic epithelial breast (MCF10A) and melanoma (MDA-MB-435) cells. The IC_{50} values obtained (including those for A549 cells) are listed in Table 3, together with those found for $\mathbf{c\text{-}Ru^{iPr}_{dmso}}$, for comparison purposes.

The Ru(II) complex $\mathbf{c\text{-}Ru^{iPr}_{dmso}}$ is more cytotoxic than $\mathbf{c\text{-}Os^{iPr}_{dmso}}$ against all cell lines tested (Table 3). Both compounds are clearly more active than the reference compound RAPTA-C, with IC_{50} values in the 1.2–4.7 μM range (*viz.*, all the complexes show high activities). It can be noted the selectivity indexes, corresponding to the ratio [IC_{50} MCF10A (non-cancerous cells)/IC_{50} MCF7 (cancerous cells)], are 0.55 and 1.08 for the Ru(II) and Os(II) complexes, respectively. Thus, $\mathbf{c\text{-}Os^{iPr}_{dmso}}$ is less toxic towards the healthy cells than $\mathbf{c\text{-}Ru^{iPr}_{dmso}}$.

Next, the effect of the phosphane R groups (Fig. 1 and 2) on the cytotoxic properties was investigated. Hence, all complexes from the ligand diphenyl(1-pyrenyl)phosphane (*i.e.*, R = Phenyl instead of isopropyl) were tested against A549 cells. The IC_{50} values obtained are given in Table 4.

It can first be stressed that the complexes with the phenyl groups are notably less active than those with the isopropyl groups (see Tables 2 and 4). As observed with the non-cyclometalated complexes bearing isopropyl groups, the osmium(II) compounds are more cytotoxic than the ruthenium(II) ones. On the contrary, for the cyclometalated compounds, the ruthenium(II) ones are more cytotoxic, although the differences in activity is less pronounced compared with those of isopropyl-containing complexes. For instance, the highest activities are again observed for the dmso-coordinated complexes $\mathbf{c\text{-}Os^{Ph}_{dmso}}$ and $\mathbf{c\text{-}Ru^{Ph}_{dmso}}$ with IC_{50} values of 6.76 and 5.17, respectively. Thus, $\mathbf{c\text{-}Ru^{Ph}_{dmso}}$ is 1.3-times more active than $\mathbf{c\text{-}Os^{Ph}_{dmso}}$ while it is 2.5 times for $\mathbf{c\text{-}Ru^{iPr}_{dmso}}$ and $\mathbf{c\text{-}Os^{iPr}_{dmso}}$. The R groups of the 1-pyrenyl-based phosphane ligand do affect the cytotoxic properties.[25]

The observed toxicity variations between the R = Ph and R = iPr complexes may result from solubility differences. Therefore, the lipophilic character of $\mathbf{c\text{-}Os^{Ph}_{Cl}}$, $\mathbf{c\text{-}Ru^{Ph}_{Cl}}$, $\mathbf{c\text{-}Os^{iPr}_{Cl}}$, $\mathbf{c\text{-}Ru^{iPr}_{Cl}}$, $\mathbf{c\text{-}Os^{Ph}_{dmso}}$, $\mathbf{c\text{-}Ru^{Ph}_{dmso}}$, $\mathbf{c\text{-}Os^{iPr}_{dmso}}$ and $\mathbf{c\text{-}Os^{iPr}_{dmso}}$ was determined using the "shake-flask" procedure, which was used to calculate their partition coefficients in an octan-1-ol (o)/water (w) system.[39] Thus, the lipophilicity of the selected cyclometalated compounds can be expressed as the logarithm of the par-

Table 3 IC_{50} values[a] (μM) of compounds $\mathbf{c\text{-}Os^{iPr}_{dmso}}$ and $\mathbf{c\text{-}Ru^{iPr}_{dmso}}$ in A549, MCF7 (breast adenocarcinoma), MCF10A (non-tumorigenic epithelial breast) and MDA-MB-435 (melanoma) human cells, after incubation of 24 h, using freshly prepared stock solutions of the complexes

Complex	A549	MCF7	MCF10A	MDA-MB-435
$\mathbf{c\text{-}Os^{iPr}_{dmso}}$	4.3 ± 0.3	4.4 ± 1.0	4.7 ± 0.7	2.3 ± 0.2
$\mathbf{c\text{-}Ru^{iPr}_{dmso}}$	1.7 ± 0.7	2.7 ± 0.5	1.5 ± 0.6	1.2 ± 0.2

[a] The results are expressed as mean values ± SD out of three independent experiments.

Table 2 Half-maximum inhibitory concentrations[a] (IC50, μM) of compounds $\mathbf{Os^{iPr}_{Cl2}}$, $\mathbf{Os^{iPr}_{I2}}$, $\mathbf{c\text{-}Os^{iPr}_{Cl}}$, $\mathbf{c\text{-}Os^{iPr}_{I}}$ and $\mathbf{c\text{-}Os^{iPr}_{dmso}}$ and the corresponding ruthenium complexes reported earlier[27] for A549 (lung adenocarcinoma) human cells, after incubation of 24 h, using freshly prepared stock solutions of the complexes

Os complex	IC_{50}	Ru Complex	IC_{50}[b]
$\mathbf{Os^{iPr}_{Cl2}}$	17.3 ± 4.6	$\mathbf{Ru^{iPr}_{Cl2}}$	24 ± 1
$\mathbf{Os^{iPr}_{I2}}$	1.4 ± 0.3[c]	$\mathbf{Ru^{iPr}_{I2}}$	48 ± 8
$\mathbf{c\text{-}Os^{iPr}_{Cl}}$	6.0 ± 0.9	$\mathbf{c\text{-}Ru^{iPr}_{Cl}}$	2.3 ± 0.3
$\mathbf{c\text{-}Os^{iPr}_{I}}$	18.8 ± 5.0	$\mathbf{c\text{-}Ru^{iPr}_{I}}$	5.8 ± 1.9
$\mathbf{c\text{-}Os^{iPr}_{dmso}}$	4.3 ± 0.3	$\mathbf{c\text{-}Ru^{iPr}_{dmso}}$	1.7 ± 0.7

[a] The results are expressed as mean values ± SD out of three independent experiments. [b] Values reported earlier.[27] [c] $\mathbf{Os^{iPr}_{I2}}$ appears to affect the cell cycle.

Table 4 IC_{50} values[a] (μM) of compounds $\mathbf{Os^{Ph}_{Cl2}}$, $\mathbf{Os^{Ph}_{I2}}$, $\mathbf{c\text{-}Os^{Ph}_{Cl}}$, $\mathbf{c\text{-}Os^{Ph}_{I}}$ and $\mathbf{c\text{-}Os^{Ph}_{dmso}}$ and the corresponding ruthenium complexes in A549 cells, after incubation of 24 h, using freshly prepared stock solutions of the complexes

Os complex	IC_{50}	Ru complex	IC_{50}
$\mathbf{Os^{Ph}_{Cl2}}$	37.3 ± 5.7	$\mathbf{Ru^{Ph}_{Cl2}}$	74.7 ± 2.3[b]
$\mathbf{Os^{Ph}_{I2}}$	>10[c]	$\mathbf{Ru^{Ph}_{I2}}$	>10
$\mathbf{c\text{-}Os^{Ph}_{Cl}}$	>50	$\mathbf{c\text{-}Ru^{Ph}_{Cl}}$	>50
$\mathbf{c\text{-}Os^{Ph}_{I}}$	>10[c]	$\mathbf{c\text{-}Ru^{Ph}_{I}}$	7.9 ± 0.7
$\mathbf{c\text{-}Os^{Ph}_{dmso}}$	6.8 ± 2.0	$\mathbf{c\text{-}Ru^{Ph}_{dmso}}$	5.2 ± 1.0

[a] The results are expressed as mean values ± SD out of three independent experiments. [b] Value reported earlier.[25] [c] Not tested with concentrations higher than 10 μM due to solubility limitations.

tition coefficients using these solvents ($\log P_{o/w}$), which can be estimated using eqn (1):

$$\log P_{O/W} = \log\left(\frac{A_{cs}}{A_{fs} - A_{cs}}\right) \quad (1)$$

where A_{fs} is the absorption value corresponding to the maximum absorption band of the compound after partition in water saturated with octan-1-ol and A_{cs} is the absorption value after subsequent partition in octan-1-ol saturated with water. The corresponding UV-Vis spectra are shown in Fig. S68.† From these spectroscopic data (experiments carried out in triplicate), $\log P_{o/w}$ values could be obtained for the eight complexes (Table S7†). The positive values obtained characterize a lipophilic character. Though, in all cases, the complexes bearing a R = iPr group are less lipophilic than the R = Ph ones; hence, the $\log P_{o/w}$ values are about 15% lower for the chloride complexes and about 5% lower for the dmso complexes (Table S7†). Consequently, the comparatively higher hydrophobicity of the R = Ph complexes may explain, at least in part, their lower cytotoxicity.

As mentioned above, $\mathbf{Os_{I2}^{iPr}}$ exhibited the lowest IC_{50} value with A549 cells. However, in contrast to $\mathbf{Os_{Cl2}^{iPr}}$, $\mathbf{c\text{-}Os_{Cl}^{iPr}}$, $\mathbf{c\text{-}Os_{I}^{iPr}}$, $\mathbf{c\text{-}Os_{dmso}^{iPr}}$, $\mathbf{Os_{Cl2}^{Ph}}$, $\mathbf{c\text{-}Os_{dmso}^{Ph}}$ (Tables 2 and 4), $\mathbf{Os_{I2}^{iPr}}$ did not induce a decrease in cell viability of more than 55%, even at the highest concentrations used; actually, few dead cells were observed. This behaviour suggested that $\mathbf{Os_{I2}^{iPr}}$ was affecting the cell cycle. Therefore, cell-cycle analyses by quantifying the DNA content with flow cytometry were carried out in A549 cells by incubating them for 48 h with 5 μM $\mathbf{Os_{I2}^{iPr}}$ and with 10 μM $\mathbf{Os_{I2}^{Ph}}$ (negative control). The corresponding results as the percentage of cells in the G_0/G_1 (pre-initiation of DNA replication), S (DNA replication), and G_2/M (post-replication, initiation of cell division/mitosis) phases of the cell cycle are listed in Table S8† and illustrated in Fig. 5 and S69.† The observed debris population was gated mainly as a subdiploid population and is related to cell death.

As anticipated, $\mathbf{Os_{I2}^{iPr}}$ clearly affects the cell cycle of A549 cells. This compound significantly arrests the cycle at the G_0/G_1 phase (68% of the cells at this phase *vs.* 60% for the control). Due to G_0/G_1 phase blockade, statistically significant lower percentages of cells in the S and G_2/M phases were observed compared to the control groups (9 *vs.* 17% and 11 *vs.* 20%, respectively). Thus, DNA production is reduced in the presence of $\mathbf{Os_{I2}^{iPr}}$; hence, cell division is hampered by this compound and the observed IC_{50} value of 1.42 μM (Table 2) is most likely not solely due to cell death (approximately 12%, debris population) but also to a significant reduction of cell division. When the isopropyl groups of the phosphane ligand are replaced by phenyl ones, the resulting complex, *viz.* $\mathbf{Os_{I2}^{Ph}}$, does not affect at all the cell cycle showing values like those of the control groups. These cell-cycle data again show that the R groups of the phosphane ligand influence the behaviour of the corresponding compounds towards the cells. To discard that the lack of effect of $\mathbf{Os_{I2}^{Ph}}$ on cell viability is caused by a restricted entrance of the compound inside the cell, live-cell imaging with confocal microscopy was carried out. It could be noticed that, despite its low fluorescence intensity, $\mathbf{Os_{I2}^{Ph}}$ can enter the cell and is localized in all the cell cytoplasm, and mainly accumulates inside lysosomes after 3 h of treatment (Fig. S70†).

In summary, all the Os(II) compounds with isopropyl groups showed higher effects on cell viability than the corresponding compounds with phenyl groups. Moreover, although $\mathbf{Os_{I2}^{iPr}}$ showed the lowest IC_{50} value (namely, 1.42 μM), its effect is not only due to toxicity, but also to cell-cycle arrest. In contrast, the other Os(II) compounds with isopropyl groups were cytotoxic, $\mathbf{c\text{-}Os_{dmso}^{iPr}}$ being the most potent one (IC_{50} = 4.26 μM).

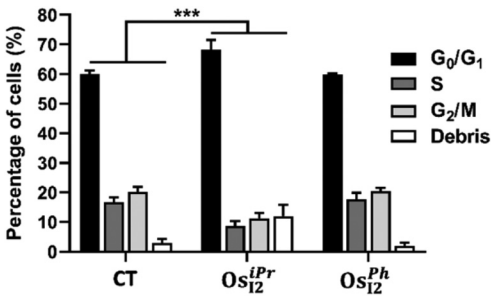

Fig. 5 Cell cycle distribution of A549 cells after 48 h treatment with $\mathbf{Os_{I2}^{iPr}}$ and $\mathbf{Os_{I2}^{Ph}}$ in the G_0/G_1, S and G_2/M phases, using flow cytometry. The Debris state was characterised mainly as a subdiploid population related to cell death. The data are presented as mean ± standard deviation. One-way ANOVA with Dunnett *post hoc* analysis was used to analyse the differences between treated cells and non-treated control groups (CT). ***$p < 0.001$.

Experimental

General considerations

All compounds were prepared under a purified dinitrogen atmosphere using standard *Schlenk* and vacuum-line techniques. The solvents were purified by a solvent purification system or by standard procedures[40] and stored under dinitrogen. ^{1}H, $^{13}C\{^{1}H\}$, $^{31}P\{^{1}H\}$, ^{1}H–^{13}C HSQC NMR spectra were recorded at room temperature with 400 or 500 MHz spectrometers. Chemical shifts are reported downfield from standards and the coupling constants are given in Hz. The IR spectra were recorded using Attenuated Total Reflection (ATR) and the main absorption bands are expressed in cm^{-1}. High-resolution mass analyses (HRMS) were carried out using electrospray ionisation (ESI). The metallic dimers of formula [MX(μ-X)(η^6-*p*-cymene)]$_2$ (M = Ru, Os; X = Cl, I)[41–45] and diphosphane ligands $\mathbf{PPyriPr_2}$[27] and $\mathbf{PPyrPh_2}$[25] were prepared following reported procedures.

Synthesis

Preparation of the osmium compounds

[$OsCl_2$(η^6-p-cymene)(diisopropyl(1-pyrenyl)phosphane)] ($\mathbf{Os_{Cl2}^{iPr}}$). A suspension of [OsCl(μ-Cl)(η^6-*p*-cymene)]$_2$ (79 mg, 0.10 mmol) and $\mathbf{PPyriPr_2}$ (96 mg, 0.30 mmol; 1.5 equiv.) in 5 mL of dichloromethane was stirred for 24 h at room temperature. The

solvent was subsequently removed under reduced pressure and the crude product was recrystallized in dichloromethane/hexane at −20 °C. The crystalline compound was filtered and washed with pentane. $\mathbf{Os^{iPr}_{Cl2}}$ was obtained as a yellow solid with a yield of 83% (119 mg). $^{31}P\{^1H\}$ NMR (162 MHz, $CDCl_3$) δ/ppm: −4.3 (s) (Fig. S12†). ^1H NMR (400 MHz, $CDCl_3$) δ/ppm: 8.79 (d, J = 9.2, $1H_{Ar}$), 8.46 (t, J = 10.0, $1H_{Ar}$), 8.31–8.08 (m, $7H_{Ar}$), 5.57 (br, s, 1H), 5.22 (br, s, 1H), 5.02 (br, s, 1H), 4.40 (br, s, 1H), 4.00 (br, s, 1H), 3.48 (br, s, 1H), 2.89 (hept, J = 6.8, $1H_{Ar}$), 1.80 (br, s, 3H), 1.67 (br, s, 3H), 1.58 (s, 3H), 1.29–1.20 (m, 9H), 0.64 (br, s, 3H) (Fig. S13 and S14†). $^{13}C\{^1H\}$ NMR (101 MHz, $CDCl_3$) δ/ppm: 133.8–123.8 (m, C_{Ar}, CH_{Ar}), 104.8 (d, J_{CP} = 4.8, C, *p*-cymene), 90.3 (s, C, *p*-cymene), 81.7 (s, CH, *p*-cymene), 78.7 (s, CH, *p*-cymene), 76.3 (s, 2CH, *p*-cymene), 30.5 (s, CH_3), 23.3–17.9 (m, CH, CH_3) (Fig. S14 and S15†). FTIR (ATR, neat) ν/cm^{-1}: 3038, 2962, 2925, 2869, 1581, 1377, 1204, 1023, 851, 644. HRMS (TOF AP(+))/m/z: $[M - 2Cl - H]^+$; calcd for $C_{32}H_{36}OsP$ 643.2169. Found 643.2167. Anal. calcd for $C_{32}H_{37}Cl_2OsP$: C, 53.85%; H, 5.23%. Found: C, 52.34%; H, 5.34%.

[OsI$_2$(η^6-p-cymene)(diisopropyl(1-pyrenyl)phosphane)] ***(Os^{iPr}_{I2}).*** $\mathbf{Os^{iPr}_{Cl2}}$ (101 mg, 0.14 mmol) and sodium iodide (300 mg, 2.00 mmol) were suspended in 20 mL of technical acetone. The reaction mixture was refluxed for 1 h and the resulting dark suspension was evaporated under reduced pressure. The residue was extracted with dichloromethane (3 × 10 mL) and water (10 mL). The combined organic phase was dried with anhydrous sodium sulfate, filtered and the solvent was removed under reduced pressure. The crude compound was recrystallized in dichloromethane/hexane at −20 °C. The crystalline compound was subsequently isolated and washed with pentane. $\mathbf{Os^{iPr}_{I2}}$ was obtained as a pale orange solid with a yield of 49% (62 mg). $^{31}P\{^1H\}$ NMR (162 MHz, $CDCl_3$) δ/ppm: −16.7 (s) (Fig. S16†). ^1H NMR (400 MHz, $CDCl_3$) δ/ppm: 8.87 (d, J = 9.5, $1H_{Ar}$), 8.43 (t, J = 8.5, $1H_{Ar}$), 8.31–8.08 (m, $7H_{Ar}$), 5.63 (br, s, 1H), 5.14 (br, s, 1H), 5.03 (br, s, 1H), 4.48 (br, s, 1H), 4.35 (br, s, 1H), 3.61 (br, s, 1H), 3.24 (hept, J = 6.5, 1H), 1.87 (dd, J = 16.5, 7.5, 3H), 1.71 (br, s, 3H), 1.66 (t, J = 8.0, 3H), 1.50 (dd, J = 11.0, 5.0, 3H), 1.26 (br, s, 3H), 1.03 (d, J = 7.0, 3H), 0.62 (br, s, 3H) (Fig. S17 and S18†). $^{13}C\{^1H\}$ NMR (101 MHz, $CDCl_3$) δ/ppm: 132.8–123.2 (m, C_{Ar}, CH_{Ar}), 105.0 (s, C, *p*-cymene), 92.4 (s, C, *p*-cymene), 80.9 (s, CH, *p*-cymene), 79.8 (s, 2CH, *p*-cymene), 79.3 (s, CH, *p*-cymene), 79.2 (s, 2CH, *p*-cymene), 30.5 (s, CH_3), 24.4–18.7 (m, CH, CH_3) (Fig. S18 and S19†). FTIR (ATR, neat) ν/cm^{-1}: 2953, 2925, 2866, 1582, 1457, 1375, 1285, 1203, 1107, 1027, 868, 753, 643, 610. HRMS (TOF AP(+))/m/z: $[M - I]^+$; calcd for $C_{32}H_{37}IOsP$ 771.1293. Found 771.1276. Anal. calcd for $C_{32}H_{37}I_2OsP$: C, 42.86%; H, 4.16%. Found: C, 42.88%; H, 4.17%.

[OsCl-(η^6-p-cymene)(k^2C-diisopropyl(1-pyrenyl)phosphane)] ***(c-Os^{iPr}_{Cl}).*** A suspension of $[OsCl(\mu\text{-}Cl)(\eta^6\text{-}p\text{-cymene})]_2$ (128 mg, 0.16 mmol), **PPyriPr$_2$** (233 mg, 0.73 mmol) and sodium acetate (77 mg, 0.94 mmol) in 40 mL of methanol was stirred for 24 h at room temperature. The solvent was removed under reduced pressure and the residue was extracted with dichloromethane (3 × 10 mL) and water (10 mL). The combined organic phase was dried with anhydrous sodium sulfate, filtered and the solvent was removed under reduced pressure. The crude product was recrystallized in dichloromethane/hexane at −20 °C. The crystalline compound was filtered and washed with pentane. **c-$\mathbf{Os^{iPr}_{Cl}}$** was obtained as a dark yellow solid with a yield of 75% (163 mg). $^{31}P\{^1H\}$ NMR (162 MHz, $CDCl_3$) δ/ppm: +39.0 (s) (Fig. S20†). ^1H NMR (400 MHz, $CDCl_3$) δ/ppm: 8.81 (s, $1H_{Ar}$), 8.11–7.92 (m, $7H_{Ar}$), 6.14 (d, J = 5.6, 1H), 6.11 (d, J = 6.0, 1H), 5.35 (d, J = 5.6, 1H), 5.05 (d, J = 5.6, 1H), 3.15–3.09 (m, 1H), 3.00–2.96 (m, 1H), 2.73 (hept, J = 7.2, 1H), 2.11 (s, 3H), 1.56 (dd, J = 14.8, 7.2, 3H), 1.41 (dd, J = 15.6, 7.2, 3H), 1.19 (d, J = 6.8, 3H), 1.11 (d, J = 7.2, 3H), 1.09–1.01 (m, 6H) (Fig. S21 and S22†). $^{13}C\{^1H\}$ NMR (101 MHz, $CDCl_3$) δ/ppm: 153.0–122.5 (m, C_{Ar}, CH_{Ar}), 100.8 (s, C, *p*-cymene), 88.4 (s, CH, *p*-cymene), 87.1 (s, C, *p*-cymene), 83.7 (s, CH, *p*-cymene), 80.1 (s, CH, *p*-cymene), 78.5 (s, CH, *p*-cymene), 30.6 (s, CH), 28.8 (d, J_{CP} = 31.7, CH), 25.3 (d, J_{CP} = 30.3, CH), 23.7 (s, CH_3), 22.8 (s, CH_3), 21.6 (s, CH_3), 19.8 (s, CH_3), 19.3 (s, CH_3), 19.0 (s, CH_3), 18.0 (s, CH_3) (Fig. S22 and S23†). FTIR (ATR, neat) ν/cm^{-1}: 2921, 2852, 1566, 1457, 1303, 1033, 868, 755, 662. HRMS (TOF AP(+))/m/z: $[M - Cl]^+$; calcd for $C_{32}H_{36}OsP$ 643.2170. Found 643.2169. Anal. calcd for $C_{32}H_{36}ClOsP$: C, 56.75%; H, 5.36% Found: C, 55.82%; H, 6.80%.

[OsI-(η^6-p-cymene)(k^2C-diisopropyl(1-pyrenyl)phosphane)] ***(c-Os^{iPr}_{I}).*** Complex **c-$\mathbf{Os^{iPr}_{Cl}}$** (163 mg, 0.24 mmol) and sodium iodide (899 mg, 6.00 mmol) were suspended in 40 mL of technical acetone. The resulting reaction mixture was refluxed for 12 h. The dark suspension was evaporated under reduced pressure and the residue was extracted with dichloromethane (3 × 10 mL) and water (10 mL). The combined organic phase was dried with anhydrous sodium sulfate, filtered and the solvent was removed under reduced pressure. The crude compound was first purified by column chromatography (silica, dichloromethane). The eluent from the fraction corresponding to the desired compound was evaporated under reduced pressure. The remaining solid was subsequently recrystallized in dichloromethane/hexane at −20 °C. The pure crystalline compound was isolated by filtration and washed with pentane. **c-$\mathbf{Os^{iPr}_{I}}$** was obtained as a pale brown solid with a yield of 24% (44 mg). $^{31}P\{^1H\}$ NMR (202 MHz, $CDCl_3$) δ/ppm: +34.6 (s) (Fig. S24†). ^1H NMR (500 MHz, $CDCl_3$) δ/ppm: 8.64 (s, $1H_{Ar}$), 8.09–7.94 (m, $7H_{Ar}$), 5.98 (d, J = 6.0, 1H), 5.93 (d, J = 6.0, 1H), 5.52 (d, J = 5.5, 1H), 5.23 (d, J = 5.5, 1H), 3.32 (br, 1H), 2.99–2.92 (m, 2H), 2.21 (s, 3H), 1.61 (dd, J = 13.0, 7.0, 3H), 1.49 (dd, J = 15.0, 7.0, 3H), 1.27 (d, J = 7.0, 3H), 1.09 (d, J = 7.0, 3H), 1.02 (dd, J = 13.5, 7.0, 3H), 0.90 (dd, J = 12.5, 7.0, 3H) (Fig. S25 and S26†). $^{13}C\{^1H\}$ NMR (125 MHz, $CDCl_3$) δ/ppm: 151.9–122.8 (m, C_{Ar}, CH_{Ar}), 102.3 (s, C, *p*-cymene), 88.3 (s, C, *p*-cymene), 87.3 (s, CH, *p*-cymene), 81.9 (s, CH, *p*-cymene), 80.9 (s, CH, *p*-cymene), 79.8 (s, CH, *p*-cymene), 30.9 (s, CH), 30.0 (d, J_{CP} = 28.4, CH), 29.3 (d, J_{CP} = 31.1, CH), 23.9 (s, CH_3), 23.2 (s, CH_3), 22.8 (s, CH_3), 19.8 (s, CH_3), 19.7 (s, CH_3), 19.1 (s, CH_3), 18.4 (s, CH_3) (Fig. S26 and S27†). FTIR (ATR, neat) ν/cm^{-1}: 3033, 2958, 2922, 2866, 1566, 1461, 1439, 1301, 1174, 1028, 855, 842, 738, 607. HRMS (TOF AP(+))/m/z: $[M - I]^+$; calcd for $C_{32}H_{36}OsP$ 643.2170. Found 643.2155. Anal. calcd for $C_{32}H_{36}IOsP$: C, 50.00%; H, 4.72% Found: C, 48.24%; H, 4.71%.

*[Os(η⁶-p-cymene)(kS-dmso)(k²C-diisopropyl(1-pyrenyl)phosphane)] PF_6 (**c-Os$^{iPr}_{dmso}$**).* Complex **c-Os$^{iPr}_{Cl}$** (73 mg, 0.11 mmol) and dimethylsulfoxide (0.1 mL, 110 mg, 1.41 mmol) were dissolved in 15 mL of dichloromethane and thallium hexafluorophosphate (45 mg, 0.13 mmol) was added. The initially transparent reaction mixture was stirred for 12 h, giving a cloudy solution. The thallium chloride obtained was removed by filtration using a filter paper and the solvent was evaporated under reduced pressure. The crude compound was recrystallized in dichloromethane/diethyl ether at −20 °C. The resulting crystalline product was isolated by filtration and washed with pentane. **c-Os$^{iPr}_{dmso}$** was obtained as a pale-yellow solid with a yield of 45% (39 mg). $^{31}P\{^1H\}$ NMR (162 MHz, $CDCl_3$) δ/ppm: +43.5 (s), −144.0 (hept, J_{PF} = 713.1) (Fig. S28†). ^1H NMR (400 MHz, $CDCl_3$) δ/ppm: 8.59 (s, $1H_{Ar}$), 8.35 (d, J = 6.8, $1H_{Ar}$), 8.21–8.05 (m, $6H_{Ar}$), 6.66 (d, J = 6.4, 1H), 6.61 (d, J = 6.0, 1H), 5.93 (s, br, 1H), 5.61 (s, br, 1H), 3.49 (s, 3H), 3.34–2.28 (m, 1H), 3.14 (hept, J = 6.8, 1H), 2.65–2.59 (m, 1H), 2.40 (s, 3H), 1.75 (s, 3H), 1.68 (dd, J = 16.0, 6.8, 3H), 1.47 (dd, J = 17.2, 6.4, 3H), 1.43 (d, J = 7.2, 3H), 1.33 (dd, J = 13.2, 6.4, 3H), 1.12 (d, J = 6.8, 3H), 0.25 (dd, J = 16.4, 6.8, 3H) (Fig. S29 and S30†). $^{13}C\{^1H\}$ NMR (101 MHz, $CDCl_3$) δ/ppm: 151.3–122.7 (m, C_{Ar}, CH_{Ar}), 88.3 (s, CH, *p*-cymene), 85.4 (s, CH, *p*-cymene), 54.7 (s, CH_3), 46.2 (s, CH_3), 31.2 (s, CH), 31.0 (d, J_{CP} = 32.7, CH), 25.9 (d, J_{CP} = 32.2, CH), 24.7 (s, CH_3), 21.4 (s, CH_3), 19.3 (s, $2CH_3$), 19.1 (s, CH_3), 18.6 (s, CH_3), 18.4 (d, J_{CP} = 5.4, CH_3) (Fig. S30 and S31†). FTIR (ATR, neat) ν/cm^{-1}: 2970, 1442, 1385, 1289, 1106, 1010, 843 ($\nu(PF_6)$), 741, 668. HRMS (TOF AP(+))/*m*/*z*: $[M - PF_6]^+$; calcd for $C_{32}H_{36}OsP$ 721.2309. Found 721.2294.

*[$OsCl_2$(η⁶-p-cymene)(diphenyl(1-pyrenyl)phosphane)] (**Os$^{Ph}_{Cl2}$**).* The procedure used to prepare **Os$^{iPr}_{Cl2}$** was followed but using $[OsCl(\mu\text{-}Cl)(\eta^6\text{-}p\text{-cymene})]_2$ (56 mg, 0.07 mmol) and **PPyrPh$_2$** (70 mg, 0.18 mmol). **Os$^{Ph}_{Cl2}$** was obtained as an orange-brown solid with a yield of 73% (80 mg). $^{31}P\{^1H\}$ NMR (162 MHz, $CDCl_3$) δ/ppm: −4.8 (s) (Fig. S32†). ^1H NMR (400 MHz, $CDCl_3$) δ/ppm: 8.91 (d, J = 9.2, $1H_{Ar}$), 8.31–8.27 (m, $2H_{Ar}$), 8.20 (d, J = 9.2, $1H_{Ar}$), 8.13–8.08 (m, $4H_{Ar}$), 7.66 (br, 4H), 7.57 (dd, J = 10.8, 8.0, $1H_{Ar}$), 7.40–7.36 (br, $2H_{Ar}$), 7.29 (br, $6H_{Ar}$), 5.43 (br, s, 2H), 4.71 (br, s, 2H), 3.00 (hept, J = 7.2, 1H), 1.74 (br, s, 3H), 1.25 (d, J = 6.8, 6H) (Fig. S33 and S34†). $^{13}C\{^1H\}$ NMR (125 MHz, $CDCl_3$) δ/ppm: 136.1–123.9 (m, C_{Ar}, CH_{Ar}), 107.5 (d, J_{CP} = 6.7, C, *p*-cymene), 90.8 (s, C, *p*-cymene), 30.4 (s, CH), 22.3 (s, $2CH_3$), 18.4 (s, CH_3) (Fig. S34 and S35†). FTIR (ATR, neat) ν/cm^{-1}: 3052, 2956, 1581, 1434, 1386, 1158, 1092, 1027, 856, 740, 690, 636, 607. HRMS (TOF AP(+))/*m*/*z*: $[M - 2Cl - H]^+$; calcd for $C_{38}H_{32}OsP$ 711.1856. Found 711.1853. Anal. calcd for $C_{38}H_{33}Cl_2OsP$: C, 58.38%; H, 4.25% Found: C, 58.22%; H, 4.27%.

*[OsI_2(η⁶-p-cymene)(diphenyl(1-pyrenyl)phosphane)] (**Os$^{ph}_{I2}$**).* The procedure used to prepare **Os$^{iPr}_{I2}$** was followed but using **Os$^{Ph}_{Cl2}$** (79 mg, 0.10 mmol) and sodium iodide (210 mg, 1.40 mmol). **Os$^{Ph}_{I2}$** was obtained as an orange solid with a yield of 75% (72 mg). $^{31}P\{^1H\}$ NMR (162 MHz, $CDCl_3$) δ/ppm: −20.2 (s) (Fig. S36†). ^1H NMR (400 MHz, $CDCl_3$) δ/ppm: 8.80 (br, s, $1H_{Ar}$), 8.28 (d, J = 7.6, $1H_{Ar}$), 8.24 (d, J = 8.0, $1H_{Ar}$), 8.19 (d, J = 8.8, $1H_{Ar}$), 8.13–8.01 (m, $5H_{Ar}$), 7.70 (br, $5H_{Ar}$), 7.33 (br, $5H_{Ar}$), 5.58 (br, 2H), 5.08–4.50 (br, 2H), 3.43 (hept, J = 6.8, 1H), 1.78 (s, 3H), 1.23 (d, J = 6.8, 6H) (Fig. S37 and S38†). $^{13}C\{^1H\}$ NMR (101 MHz, $CDCl_3$) δ/ppm: 133.7–123.8 (m, C_{Ar}, CH_{Ar}), 106.7 (d, J_{CP} = 6.3, C, *p*-cymene), 93.2 (s, C, *p*-cymene), 31.9 (s, $2CH_3$), 31.7 (s, CH), 18.9 (s, CH_3) (Fig. S38 and S39†). FTIR (ATR, neat) ν/cm^{-1}: 3037, 2957, 2865, 1582, 1433, 1370, 1207, 1181, 1090, 1022, 851, 752, 689, 631. HRMS (TOF AP(+))/*m*/*z*: $[M - I]^+$; calcd for $C_{38}H_{33}IOsP$ 839.0979. Found 839.0976. Anal. calcd for $C_{38}H_{33}I_2OsP$: C, 47.31%; H, 3.45% Found: C, 46.99%; H, 3.78%.

*[OsCl-(η⁶-p-cymene)(k²C-diphenyl(1-pyrenyl)phosphane)] (**c-Os$^{Ph}_{Cl}$**).* The procedure used to prepare **c-Os$^{iPr}_{Cl}$** was applied but using $[OsCl(\mu\text{-}Cl)(\eta^6\text{-}p\text{-cymene})]_2$ (126 mg, 0.16 mmol), **PPyrPh$_2$** (286 mg, 0.74 mmol) and sodium acetate (77 mg, 0.94 mmol). **c-Os$^{iPr}_{Cl}$** was obtained as a dark yellow solid with a yield of 97% (231 mg). $^{31}P\{^1H\}$ NMR (202 MHz, $CDCl_3$) δ/ppm: +28.5 (s) (Fig. S40†). ^1H NMR (500 MHz, $CDCl_3$) δ/ppm: 8.84 (s, $1H_{Ar}$), 8.18–8.05 (m, $9H_{Ar}$), 7.98 (t, J = 7.5, $1H_{Ar}$), 7.73–7.41 (m, $4H_{Ar}$), 7.34–7.32 (m, $3H_{Ar}$), 7.22–7.19 (m, $2H_{Ar}$), 5.90 (d, J = 6.0, 1H), 5.81 (d, J = 5.5, 1H), 4.77 (d, J = 5.5, 1H), 4.55 (d, J = 5.5, 1H), 2.35 (hept, J = 7.0, 1H), 2.11 (s, 3H), 1.03 (d, J = 7.0, 3H), 0.73 (d, J = 7.0, 3H) (Fig. S41 and S42†). $^{13}C\{^1H\}$ NMR (125 MHz, $CDCl_3$) δ/ppm: 152.8–122.9 (m, C_{Ar}, CH_{Ar}), 98.4 (s, C, *p*-cymene), 91.3 (s, C, *p*-cymene), 86.3 (d, J_{CP} = 3.4, CH, *p*-cymene), 84.9 (d, J_{CP} = 5.3, CH, *p*-cymene), 84.7 (d, J_{CP} = 5.9, CH, *p*-cymene), 78.5 (d, J_{CP} = 4.5, CH, *p*-cymene), 30.0 (s, CH), 22.9 (s, CH_3), 22.7 (s, CH_3), 18.0 (s, CH_3) (Fig. S42 and S43†). FTIR (ATR, neat) ν/cm^{-1}: 3035, 2956, 1581, 1480, 1433, 1381, 1305, 1181, 1095, 1028, 846, 752, 601. HRMS (TOF AP(+))/*m*/*z*: $[M - Cl]^+$; calcd for $C_{38}H_{32}OsP$ 711.1857. Found 711.1847. Anal. calcd for $C_{38}H_{32}ClOsP$: C, 61.24%; H, 4.33% Found: C, 61.69%; H, 4.35%.

*[OsI-(η⁶-p-cymene)(k²C-diphenyl(1-pyrenyl)phosphane)] (**c-Os$^{Ph}_{I}$**).* A suspension of $[OsI(\mu\text{-}I)(\eta^6\text{-}p\text{-cymene})]_2$ (88 mg, 0.08 mmol), **PPyrPh$_2$** (88 mg, 0.23 mmol) and sodium acetate (50 mg, 0.61 mmol) in 25 mL of methanol was stirred for 12 h at room temperature. The solvent was removed under reduced pressure and the residue was extracted with dichloromethane (3 × 10 mL) and water (10 mL). The combined organic phase was dried with anhydrous sodium sulfate, filtered and the filtrate was evaporated under reduced pressure. The crude was recrystallized in dichloromethane/diethyl ether at −20 °C. The pure crystalline compound was isolated by filtration and washed with pentane. **c-Os$^{Ph}_{I}$** was obtained as an olive-green solid with a yield of 46% (61 mg). $^{31}P\{^1H\}$ NMR (202 MHz, $CDCl_3$) δ/ppm: +24.1 (s) (Fig. S44†). ^1H NMR (500 MHz, $CDCl_3$) δ/ppm: 8.70 (s, $1H_{Ar}$), 8.18–7.96 (m, $9H_{Ar}$), 7.45–7.40 (m, $4H_{Ar}$), 7.30–7.26 (m, $3H_{Ar}$), 7.18–7.14 (m, $2H_{Ar}$), 5.70 (d, J = 6.0, 1H), 5.60 (d, J = 7.2, 1H), 4.93 (d, J = 6.0, 1H), 4.58 (d, J = 5.6, 1H), 2.64 (hept, J = 7.2, 1H), 2.27 (s, 3H), 1.13 (d, J = 6.8, 3H), 0.66 (d, J = 7.2, 3H) (Fig. S45 and S46†). $^{13}C\{^1H\}$ NMR (125 MHz, $CDCl_3$) δ/ppm: 153.2–122.7 (m, C_{Ar}, CH_{Ar}), 101.2 (s, C, *p*-cymene), 90.1 (s, C, *p*-cymene), 86.4 (d, J_{CP} = 5.1, CH, *p*-cymene), 86.0 (d, J_{CP} = 3.6, CH, *p*-cymene), 82.9 (d, J_{CP} = 5.6, CH, *p*-cymene), 78.4 (d, J_{CP} = 4.1, CH, *p*-cymene), 30.5 (s, CH), 23.1 (s, CH_3), 22.3 (s, CH_3), 19.0 (s, CH_3) (Fig. S46 and S47†). FTIR (ATR, neat) ν/cm^{-1}:

3038, 2956, 2919, 2865, 1566, 1459, 1433, 1381, 1304, 1180, 1094, 1030, 846, 754, 693, 619. HRMS (TOF AP(+))/*m*/*z*: [M − I]$^+$; calcd for $C_{38}H_{32}OsP$ 711.1857. Found 711.1848. Anal. calcd for $C_{38}H_{32}IOsP$: C, 54.54%; H, 3.85% Found: C, 54.99%; H, 4.01%.

*[Os(η^6-p-cymene)(kS-dmso)(k^{2}C-diphenyl(1-pyrenyl)phosphane)] PF_6 (**c-Os$^{Ph}_{dmso}$**).* The procedure used to prepare **c-Os$^{iPr}_{dmso}$** was followed but using **c-Os$^{Ph}_{Cl}$** (101 mg, 0.14 mmol), dimethylsulfoxide (0.1 mL, 110 mg, 1.41 mmol) and thallium hexafluorophosphate (65 mg, 0.19 mmol). The reaction mixture was stirred for 2.5 h at room temperature. **c-Os$^{Ph}_{dmso}$** was obtained as a pale-green solid with a yield of 68% (89 mg). ^{31}P{^{1}H} NMR (162 MHz, $CDCl_3$) δ/ppm: +28.1 (s), −144.2 (hept, J_{PF} = 714.4) (Fig. S48†). ^{1}H NMR (400 MHz, $CDCl_3$) δ/ppm: 8.77 (s, 1H$_{Ar}$), 8.51 (d, J = 7.6, 1H$_{Ar}$), 8.32–8.13 (m, 7H$_{Ar}$), 7.88 (m, 1H$_{Ar}$), 7.64–7.63 (m, 3H$_{Ar}$), 7.45–7.33 (m, 4H$_{Ar}$), 6.48 (d, J = 5.6, 1H), 5.99 (d, J = 6.0, 1H), 5.73 (d, J = 6.0, 1H), 4.57 (d, J = 6.4, 1H), 3.44 (s, 3H), 2.87 (hept, J = 6.8, 1H), 2.51 (s, 3H), 1.76 (s, 3H), 1.24 (d, J = 7.2, 3H), 0.95 (d, J = 6.8, 3H) (Fig. S49 and S50†). ^{13}C{^{1}H} NMR (125 MHz, $CDCl_3$) δ/ppm: 143.3–125.2 (m, C$_{Ar}$, CH$_{Ar}$), 119.4 (s, C, *p*-cymene), 106.7 (s, C, *p*-cymene), 93.4 (s, CH, *p*-cymene), 90.4 (d, J_{CP} = 3.4, CH, *p*-cymene), 86.3 (d, J_{CP} = 5.3, CH, *p*-cymene), 81.5 (d, J_{CP} = 5.9, CH, *p*-cymene), 52.8 (s, CH_3), 41.2 (s, CH_3), 30.5 (s, CH), 23.7 (s, CH_3), 20.4 (s, CH_3), 19.0 (s, CH_3) (Fig. S50 and S51†). FTIR (ATR, neat) ν/cm^{-1}: 2972, 1568, 1472, 1437, 1387, 1292, 1183, 1097, 1013, 843 (ν(PF_6)), 694, 606. HRMS (TOF AP(+))/*m*/*z*: [M − PF_6]$^+$; calcd for $C_{40}H_{38}OPOsS$ 789.1996. Found 789.1979.

Preparation of the ruthenium compounds

*[RuI$_2$(η^6-p-cymene)(diphenyl(1-pyrenyl)phosphane)] (**Ru$^{Ph}_{I2}$**).* The procedure used to prepare **Os$^{iPr}_{I2}$** was followed but using **Ru$^{Ph}_{Cl2}$** (450 mg, 0.65 mmol) and sodium iodide (1500 mg, 10.00 mmol). **Ru$^{Ph}_{I2}$** was obtained as a dark brown solid with a yield of 65% (369 mg). ^{31}P{^{1}H} NMR (162 MHz, $CDCl_3$) δ/ppm: +23.1 (s) (Fig. S52†). ^{1}H NMR (400 MHz, $CDCl_3$) δ/ppm: 8.61 (br, s, 1H$_{Ar}$), 8.28 (d, J = 7.6, 1H$_{Ar}$), 8.23–8.04 (m, 7H$_{Ar}$), 7.95 (d, J = 9.6, 1H$_{Ar}$), 7.73 (br, s, 4H$_{Ar}$), 7.35 (br, 5H$_{Ar}$), 5.43 (br, s, 2H), 4.71 (br, s, 2H), 3.53 (hept, J = 6.8, 1H), 1.79 (s, 3H), 1.23 (br, s, 6H) (Fig. S53 and S54†). ^{13}C{^{1}H} NMR (101 MHz, $CDCl_3$) δ/ppm: 135.2–123.7 (m, C$_{Ar}$, CH$_{Ar}$), 112.8 (d, J_{CP} = 6.1, C, *p*-cymene), 100.8 (s, C, *p*-cymene), 88.6 (d, J_{CP} = 4.5, CH, *p*-cymene), 88.1 (br, s, CH, *p*-cymene), 32.1 (s, CH), 22.8 (br, s, 2CH_3), 19.1 (s, CH_3) (Fig. S54 and S55†). FTIR (ATR, neat) ν/cm^{-1}: 3048, 2957, 2917, 2861, 1470, 1430, 1374, 1087, 852, 687, 635. HRMS (TOF AP(+))/*m*/*z*: [M − I]$^+$; calcd for $C_{38}H_{33}IPRu$ 749.0408. Found 749.0413. Anal. calcd for $C_{38}H_{33}I_2PRu$: C, 52.13%; H, 3.80% Found: C, 51.80%; H, 3.92%.

*[RuCl-(η^6-p-cymene)(k^{2}C-diphenyl(1-pyrenyl)phosphane)] (**c-Ru$^{Ph}_{Cl}$**).* A suspension of [RuCl(μ-Cl)(η^6-*p*-cymene)]$_2$ (643 mg, 1.05 mmol), **PPyrPh$_2$** (870 mg, 2.25 mmol) and sodium acetate (492 mg, 6.00 mmol) in 160 mL of methanol was stirred for 4 h at room temperature. The solvent was removed under reduced pressure and the residue was extracted with dichloromethane (3 × 10 mL) and water (10 mL). The combined organic phase was dried with anhydrous sodium sulfate and the filtrate was evaporated under reduced pressure. The crude was recrystallized in dichloromethane/diethyl ether at −20 °C. The resulting crystalline material was isolated by filtration and washed with pentane. **c-Ru$^{Ph}_{Cl}$** was obtained as an orange solid with a yield of 57% (787 mg). ^{31}P{^{1}H} NMR (162 MHz, $CDCl_3$) δ/ppm: +66.4 (s) (Fig. S56†). ^{1}H NMR (400 MHz, $CDCl_3$) δ/ppm: 8.94 (s, 1H$_{Ar}$), 8.18–7.97 (m, 9H$_{Ar}$), 7.45–7.42 (m, 3H$_{Ar}$), 7.36–7.29 (m, 3H$_{Ar}$), 7.23–7.18 (m, 2H$_{Ar}$), 5.97 (d, J = 7.2, 1H), 5.95 (d, J = 7.2, 1H), 4.65 (d, J = 6.0, 1H), 4.60 (d, J = 6.0, 1H), 2.51 (hept, J = 6.8, 1H), 1.98 (s, 3H), 1.07 (d, J = 6.8, 3H), 0.75 (d, J = 7.2, 3H) (Fig. S57 and S58†). ^{13}C{^{1}H} NMR (101 MHz, $CDCl_3$) δ/ppm: 168.3–122.7 (m, C$_{Ar}$, CH$_{Ar}$), 108.9 (s, C, *p*-cymene), 99.2 (s, C, *p*-cymene), 95.6 (d, J_{CP} = 4.1, CH, *p*-cymene), 93.1 (d, J_{CP} = 4.9, CH, *p*-cymene), 91.9 (d, J_{CP} = 5.5, CH, *p*-cymene), 87.2 (d, J_{CP} = 4.6, CH, *p*-cymene), 30.4 (s, CH), 22.62 (s, CH_3), 22.56 (s, CH_3), 18.4 (s, CH_3) (Fig. S58 and S59†). FTIR (ATR, neat) ν/cm^{-1}: 3065, 2955, 2920, 1570, 1432, 1304, 801, 652, 600. HRMS (TOF AP(+))/*m*/*z*: [M − Cl]$^+$; calcd for $C_{38}H_{32}PRu$ 621.1285. Found 621.1298. Anal. calcd for $C_{38}H_{32}ClPRu$: C, 69.56%; H, 4.92% Found: C, 67.38%; H, 4.87%.

*[RuI-(η^6-p-cymene)(k^{2}C-diphenyl(1-pyrenyl)phosphane)] (**c-Ru$^{Ph}_{I}$**).* The procedure used to prepare **c-Os$^{Ph}_{I}$** was followed but using [RuI(μ-I)(η^6-*p*-cymene)]$_2$ (254 mg, 0.26 mmol), **PPyrPh$_2$** (290 mg, 0.75 mmol) and sodium acetate (164 mg, 2.00 mmol); the reaction mixture was stirred for 24 h at room temperature. **c-Ru$^{Ph}_{I}$** was obtained as a brown solid with a yield of 74% (287 mg). ^{31}P{^{1}H} NMR (162 MHz, $CDCl_3$) δ/ppm: +65.0 (s) (Fig. S60†). ^{1}H NMR (400 MHz, $CDCl_3$) δ/ppm: 8.78 (s, 1H$_{Ar}$), 8.18–7.96 (m, 9H$_{Ar}$), 7.45–7.40 (m, 3H$_{Ar}$), 7.30–7.26 (m, 3H$_{Ar}$), 7.15–7.10 (m, 2H$_{Ar}$), 5.77 (d, J = 5.6, 1H), 5.74 (d, J = 6.0, 1H), 4.88 (d, J = 6.4, 1H), 4.66 (d, J = 6.0, 1H), 2.78 (hept, J = 6.8, 1H), 2.15 (s, 3H), 1.15 (d, J = 6.8, 3H), 0.70 (d, J = 7.2, 3H) (Fig. S61 and S62†). ^{13}C{^{1}H} NMR (101 MHz, $CDCl_3$) δ/ppm: 164.2–122.7 (m, C$_{Ar}$, CH$_{Ar}$), 111.6 (s, C, *p*-cymene), 99.2 (s, C, *p*-cymene), 95.1 (d, J_{CP} = 4.0, CH, *p*-cymene), 93.1 (d, J_{CP} = 5.2, CH, *p*-cymene), 91.4 (d, J_{CP} = 5.3, CH, *p*-cymene), 86.7 (d, J_{CP} = 4.6, CH, *p*-cymene), 31.0 (s, CH), 23.0 (s, CH_3), 22.4 (s, CH_3), 19.3 (s, CH_3) (Fig. S62 and S63†). FTIR (ATR, neat) ν/cm^{-1}: 3045, 2954, 2866, 1570, 1468, 1433, 1385, 1302, 1173, 1091, 1027, 846, 754, 631, 604. HRMS (TOF AP(+))/*m*/*z*: [M − I]$^+$; calcd for $C_{38}H_{32}PRu$ 621.1285. Found 621.1298. Anal. calcd for $C_{38}H_{32}IPRu$: C, 61.05%; H, 4.31% Found: C, 61.26%; H, 3.70%.

*[Ru(η^6-p-cymene)(kS-dmso)(k^{2}C-diphenyl(1-pyrenyl)phosphane)] PF_6 (**c-Ru$^{Ph}_{dmso}$**).* The procedure used to prepare **c-Os$^{iPr}_{dmso}$** was followed but using **c-Ru$^{Ph}_{Cl}$** (336 mg, 0.51 mmol), dimethylsulfoxide (0.35 mL, 385 mg, 4.94 mmol) and thallium hexafluorophosphate (196 mg, 0.56 mmol). **c-Ru$^{Ph}_{dmso}$** was obtained as a yellow solid with a yield of 64% (274 mg). ^{31}P{^{1}H} NMR (162 MHz, $CDCl_3$) δ/ppm: +67.3 (s), −144.0 (hept, J_{PF} = 713.4) (Fig. S64†). ^{1}H NMR (400 MHz, $CDCl_3$) δ/ppm: 8.79 (s, 1H$_{Ar}$), 8.52 (d, J = 6.8, 1H$_{Ar}$), 8.31–8.13 (m, 8H$_{Ar}$), 7.65 (m, 3H$_{Ar}$), 7.47–7.36 (m, 3H$_{Ar}$), 7.06 (br, 2H$_{Ar}$), 6.60 (d, J = 5.2, 1H), 6.16 (d, J = 6.0, 1H), 5.81 (d, J = 6.0, 1H), 4.62 (d, J = 6.0, 1H), 3.27 (s, 3H), 2.91 (hept, J = 6.8, 1H), 2.40 (s, 3H), 1.50 (s, 3H), 1.19 (d, J = 6.8, 3H), 0.45 (d, J = 6.8, 3H) (Fig. S65 and S66†). ^{13}C{^{1}H} NMR (125 MHz, $CDCl_3$) δ/ppm: 157.7–125.3 (m, C$_{Ar}$, CH$_{Ar}$),

122.5 (s, C, *p*-cymene), 113.0 (s, C, *p*-cymene), 100.4 (s, CH, *p*-cymene), 99.3 (s, CH, *p*-cymene), 95.6 (d, J_{CP} = 5.0, CH, *p*-cymene), 89.2 (s, CH, *p*-cymene), 52.3 (s, CH_3), 44.7 (s, CH_3), 31.0 (s, CH), 23.8 (s, CH_3), 20.6 (s, CH_3), 19.2 (s, CH_3) (Fig. S66 and S67†). FTIR (ATR, neat) ν/cm^{-1}: 1570, 1479, 1436, 1314, 1184, 1094, 1014, 843 ($\nu(PF_6)$), 697, 620. HRMS (TOF AP(+))/*m*/*z*: $[M - PF_6]^+$; calcd for $C_{40}H_{38}OPRuS$ 699.1424. Found 699.1434.

X-ray crystallography

Data for compounds $\mathbf{Os^{iPr}_{Cl2}}$, $\mathbf{Os^{iPr}_{I2}}$, $\mathbf{Os^{Ph}_{Cl2}}$, $\mathbf{Os^{Ph}_{I2}}$, $\mathbf{c\text{-}Os^{Ph}_{Cl}}$, $\mathbf{c\text{-}Ru^{Ph}_{Cl}}$ and $\mathbf{c\text{-}Ru^{Ph}_{I}}$ were collected on a Bruker APEX II QUAZAR diffractometer equipped with a microfocus multilayer monochromator with Mo Kα radiation (λ = 0.71073 Å). Data for compounds $\mathbf{c\text{-}Os^{iPr}_{Cl}}$, $\mathbf{c\text{-}Os^{iPr}_{I}}$ and $\mathbf{c\text{-}Ru^{Ph}_{dmso}}$ were collected at BL13-XALOC beamline[46] of the ALBA synchrotron (λ = 0.72931 Å). Data reduction and absorption corrections were performed by using SAINT and SADABS, respectively.[47] The structures were solved using SHELXT[48] and refined by full-matrix least-squares on F^2 with SHELXL.[49] For compound $\mathbf{c\text{-}Ru^{Ph}_{dmso}}$, a void containing only diffuse electron density was analysed and taken into account with Olex2/Solvent Mask.[50] An estimated content of two diffuse lattice CH_2Cl_2 molecules per formula unit were deduced, and included in the formula. All details can be found in CCDC 2237617–2237626,† which contain the supplementary crystallographic data for this paper.

Cell viability assays

To screen the effect of all the Os(II) compounds on cell viability, the A549 human cell line (lung adenocarcinoma) was chosen. In some experiments, the MCF7 (breast adenocarcinoma), MCF10A (non-tumorigenic epithelial breast) and MDA-MB-435 (melanoma) human cell lines were used as well. For these experiments, the different cell lines were cultured in a 96-well plate (1×10^5 cells per well) for 24 h with their proper medium at 37 °C and 5% CO_2. A549, was cultured in Dulbecco's modified Eagle's medium (DMEM, Biological Industries, Beit Haemek, Israel), MCF7, MCF10A and MDA-MB-435 were maintained in DMEM/Ham's F12 [1 : 1]. All mediums were supplemented with 100 U mL^{-1} penicillin, 100 μg mL^{-1} streptomycin, and 2 mM glutamine. Moreover, A549, MCF7 and MDA-MB-435 were supplemented with 10% fetal bovine serum, whereas MCF10A was supplemented with 5% horse serum, 10 μg mL^{-1} insulin, 100 ng mL^{-1} cholera toxin, 500 ng mL^{-1} hydrocortisone and 20 ng mL^{-1} epidermal growth factor. The next day, the cells were treated with freshly prepared complex solutions at the chosen concentration range for 24 h. Subsequently, a 3-(4,5-dimethylthiazol-2-yl)-2,5-diphenyltetrazolium bromide solution (MTT) of 5 mg mL^{-1} was added and incubation was carried out for 2 h at 37 °C. The formazan crystals formed were dissolved in 100 μL of DMSO and the absorbance at 570 nm was recorded using a multiwell plate reader (Multiskan FC, Thermo Fisher Scientific Inc). The estimated half-inhibitory concentration (IC_{50}) for each compound was calculated using GraphPad Prism v8.0.1 software (Graph-Pad, San Diego, CA, USA).

Lipophilicity

The lipophilicity of selected compounds was quantified by calculating the partition coefficients in an octan-1-ol/water system using the "shake-flask" method. The complexes were suspended in milliQ water saturated with octan-1-ol. After sonicating them for 1 h at 298 K, the suspensions were shaken for 24 h using an orbital-shaker at a rate of 120 rpm. The samples were subsequently filtered with a 0.2 μm Puradisc FP 30 mm Cellulose Acetate Syringe Filter (Whatman). Some aliquots (of 4 mL) of the filtrates (*viz.*, *fs* samples) were reserved (for the UV-Vis measurements). Other aliquots of 4 mL were poured onto 4 mL of octan-1-ol saturated with milliQ water. The resulting mixtures were shaken for 24 h at 298 K. The samples were then centrifuged, and the organic phases were isolated (*viz.*, *cs* samples). UV-Vis spectra were recorded for both the *fs* and *cs* samples (Fig. S68†). The observed differences between the MLCT absorptions of the two types of samples, namely A_{fs} and A_{cs} (see ESI†), were used to calculate the $\log P_{o/w}$ values applying eqn (1). The data obtained after measurements in triplicate are listed in Table S7.†

Cell cytometry

A549 cells were seeded in a 6-well plate (2×10^5 cells per well) and incubated for 24 h at °C. Then, the cells were treated with the different Os(II) complexes. After 48 h of incubation, the cells were harvested and fixed with a cold 70% ethanol solution and were kept at −20 °C for at least 3 h following the MUSE™ Cell cycle kit (EMD Millipore, Burlington, MA, USA) manufacturer's instructions. Afterwards, the cells were incubated with the MUSE Cell cycle reagent for 30 min and examined using the flow cytometry MUSE Cell Analyzer, to characterise the different populations (G_0/G_1, S and G_2/M) depending on their DNA content. One-way ANOVA with Dunnett *post hoc* analysis was used to analyse the observed differences.

Confocal microscopy

To localize $\mathbf{Os^{Ph}_{I2}}$ inside the cells, A549 cells were cultured in 8-well sterile-Slide (Ibidi, Gräfelfing, Germany) (3×10^4 cells per well). After 24 h of incubation, the cells were treated with 50 μM $\mathbf{Os^{Ph}_{I2}}$ for 3 h. The high concentration of $\mathbf{Os^{Ph}_{I2}}$ used is due to the low fluorescence emission exhibited by this complex. To visualize the Os(II) compound, it was excited at 405 nm with a laser and the emission between 413 and 488 nm was recorded. To localize the lysosomes in the cell, Lysotracker Red (Molecular Probes, OR, USA) at a concentration of 15 nM was pre-incubated for 30 min. The images were obtained using a Carl Zeiss LSM 880 spectral confocal laser scanning microscope (Carl Zeiss Microscopy GmbH, Jena, Germany) and processed with ZEN 2 blue edition software (Zeiss). Representative images from three independent experiments are shown in Fig. S70.†

Conclusions

The present study was carried out to compare the cytotoxic properties of osmium(II) arene complexes from hindered

monophosphane ligands with those of their ruthenium(II) counterparts. We have indeed previously shown that such [$RuX_2(\eta^6$-arene)(diR(1-pyrenyl)phosphane)] exhibit interesting cytotoxic behaviours as well as chemical properties, since they can undergo cyclometalation under basic conditions, leading to organometallic compounds with distinct biological activities (compared with the parent, non-cyclometalated complexes). The effect of the metal centre, namely osmium(II) *vs.* ruthenium(II), on the properties of this family of half-sandwich complexes was investigated. Hence, 10 osmium(II) complexes were prepared from two different diR(1-pyrenyl)phosphane ligands (R = isopropyl or phenyl), halides (X = Cl or I) and DMSO (X = dmso for the cyclometalated complexes). The X-ray structures of 7 of these osmium(II) complexes were obtained; it can be pointed out here that, to the best of our knowledge, solid-state structures of cycloosmated half-sandwich complexes have not been reported so far. To be able to perform a complete comparison with all ruthenium(II) analogues, 4 ruthenium(II) complexes were also prepared; the other 6 compounds to complete the series were reported earlier. The crystal structures of 3 of these new ruthenium(II) complexes were obtained.

The cytotoxic behaviours of the two related metallic series revealed some interesting features. The toxicity of the non-cyclometalated osmium(II) compounds is higher than the corresponding ruthenium(II) complexes, with IC_{50} values down to 1.42 μM for A549 cells (while the lowest value is 24 μM for ruthenium). Notably, the osmium(II) complexes do not undergo rapid cyclometalation in DMSO contrary to the ruthenium(II) ones, indicating that the reactivity of Os(II) is slower than that of Ru(II), as one would have expected it.[30] Indeed, as shown in a previous study, as soon as they are dissolved in DMSO, such ruthenium(II) complexes progressively convert into cyclometalated **c-Ru$^{R}_{X}$** species through a multi-step process.[27] Therefore, the cytotoxic activity of "pure" ruthenium (II) compounds of the type **Ru$^{R}_{X2}$** cannot be determined and it appears that the intermediate species are not very active. For the **Os$^{R}_{X2}$** complexes, their cytotoxic properties can be determined since their multi-step conversion towards the formation of **c-Os$^{R}_{X}$** is significantly slower. Regarding the cyclometalated complexes, while the ruthenium ones are very active in various cell lines (IC_{50} values between 2.61 and 1.19 μM), the osmium ones are comparatively less toxic (IC_{50} values between 4.36 and 2.32 μM); the cycloosmated compounds are twice less active but are still quite cytotoxic with IC_{50} < 5 μM. Again, the observed difference may be ascribed to the distinct activity of ruthenium compared with osmium, the latter being usually more inert than the former. It can also be stressed that cell-cycle studies have shown that the highest activity, *viz.* lowest IC_{50} value, exhibited by **Os$^{iPr}_{I2}$** with A549 cells is not solely due to its cytotoxicity but also to its ability to arrest the cell cycle, which is an interesting property regarding the possibility to stop tumour growth. It has been shown as well that the non-activity exhibited by **Os$^{Ph}_{I2}$** does not arise from its inability to enter A549 cells, therefore illustrating the importance of the R group of the diR(1-pyrenyl)phosphane ligand, namely phenyl *vs.* isopropyl, regarding the corresponding biological properties.

Conflicts of interest

There are no conflicts to declare.

Acknowledgements

Financial support from the Spanish Ministerio de Ciencia e Innovación (Projects PID2020-115537RB-I00, PID2020-115658GB-I00 and RED2018-102471-T; MCIN/AEI/10.13039/501100011033), the RSC (RSC Research Fund grant RF19-7147) and the AGAUR (Project 2021-SGR-01107) is kindly acknowledged. P. G. thanks the Institució Catalana de Recerca i Estudis Avançats (ICREA). This research used resources of the ALBA synchrotron. The corresponding crystallographic measurements were performed with the collaboration of ALBA staff at BL13-XALOC beamline. Dr Olivier Roubeau is thanked for his help to solve some of the crystal structures.

References

1 A. Gandioso, K. Purkait and G. Gasser, *Chimia*, 2021, **75**, 845–855.
2 S. Sen, M. Won, M. S. Levine, Y. Noh, A. C. Sedgwick, J. S. Kim, J. L. Sessler and J. F. Arambula, *Chem. Soc. Rev.*, 2022, **51**, 1212–1233.
3 C. Q. Yu, Z. B. Wang, Z. R. Sun, L. Zhang, W. W. Zhang, Y. G. Xu and J. J. Zhang, *J. Med. Chem.*, 2020, **63**, 13397–13412.
4 C. Sonkar, S. Sarkar and S. Mukhopadhyay, *RSC Med. Chem.*, 2022, **13**, 22–38.
5 A. Casini, A. Vessières and S. M. Meier-Menches, *Metal-based Anticancer Agents*, The Royal Society of Chemistry, 2019.
6 R. A. Alderden, M. D. Hall and T. W. Hambley, *J. Chem. Educ.*, 2006, **83**, 728–734.
7 S. Thota, D. A. Rodrigues, D. C. Crans and E. J. Barreiro, *J. Med. Chem.*, 2018, **61**, 5805–5821.
8 D. A. Smithen, H. M. Yin, M. H. R. Beh, M. Hetu, T. S. Cameron, S. A. McFarland and A. Thompson, *Inorg. Chem.*, 2017, **56**, 4121–4132.
9 C. G. Hartinger, S. Zorbas-Seifried, M. A. Jakupec, B. Kynast, H. Zorbas and B. K. Keppler, *J. Inorg. Biochem.*, 2006, **100**, 891–904.
10 G. Suss-Fink, *Dalton Trans.*, 2010, **39**, 1673–1688.
11 M. Zaki, S. Hairat and E. S. Aazam, *RSC Adv.*, 2019, **9**, 3239–3278.
12 P. Moharana, D. Ghosh and P. Paira, *Inorg. Chem. Commun.*, 2021, **124**, 18.
13 A. Habtemariam, M. Melchart, R. Fernandez, S. Parsons, I. D. H. Oswald, A. Parkin, F. P. A. Fabbiani, J. E. Davidson,

A. Dawson, R. E. Aird, D. I. Jodrell and P. J. Sadler, *J. Med. Chem.*, 2006, **49**, 6858–6868.
14 T. Nabiyeva, C. Marschner and B. Blom, *Eur. J. Med. Chem.*, 2020, **201**, 112483.
15 M. Hanif, M. V. Babak and C. G. Hartinger, *Drug Discovery Today*, 2014, **19**, 1640–1648.
16 G. Muhlgassner, C. Bartel, W. F. Schmid, M. A. Jakupec, V. B. Arion and B. K. Keppler, *J. Inorg. Biochem.*, 2012, **116**, 180–187.
17 C. C. Konkankit, S. C. Marker, K. M. Knopf and J. J. Wilson, *Dalton Trans.*, 2018, **47**, 9934–9974.
18 S. M. Meier-Menches, C. Gerner, W. Berger, C. G. Hartinger and B. K. Keppler, *Chem. Soc. Rev.*, 2018, **47**, 909–928.
19 A. F. A. Peacock, S. Parsons and P. J. Sadler, *J. Am. Chem. Soc.*, 2007, **129**, 3348–3357.
20 J. Hildebrandt, N. Hafner, D. Kritsch, H. Gorls, M. Durst, I. B. Runnebaum and W. Weigand, *Int. J. Mol. Sci.*, 2022, **23**, 29.
21 A. Gatti, A. Habtemariam, I. Romero-Canelon, J. I. Song, B. Heer, G. J. Clarkson, D. Rogolino, P. J. Sadler and M. Carcelli, *Organometallics*, 2018, **37**, 891–899.
22 J. Maksimoska, D. S. Williams, G. E. Atilla-Gokcumen, K. S. M. Smalley, P. L. Carroll, R. D. Webster, P. Filippakopoulos, S. Knapp, M. Herlyn and E. Meggers, *Chem. – Eur. J.*, 2008, **14**, 4816–4822.
23 A. C. Matsheku, M. Y. H. Chen, S. Jordaan, S. Prince, G. S. Smith and B. C. E. Makhubela, *Appl. Organomet. Chem.*, 2017, **31**, 14.
24 W. F. Schmid, R. O. John, V. B. Arion, M. A. Jakupec and B. K. Keppler, *Organometallics*, 2007, **26**, 6643–6652.
25 R. F. Brissos, P. Clavero, A. Gallen, A. Grabulosa, L. A. Barrios, A. B. Caballero, L. Korrodi-Gregorio, R. Perez-Tomas, G. Muller, V. Soto-Cerrato and P. Gamez, *Inorg. Chem.*, 2018, **57**, 14786–14797.
26 L. Rafols, S. Torrente, D. Aguila, V. Soto-Cerrato, R. Perez-Tomas, P. Gamez and A. Grabulosa, *Organometallics*, 2020, **39**, 2959–2971.
27 L. Rafols, D. Josa, D. Aguila, L. A. Barrios, O. Roubeau, J. Cirera, V. Soto-Cerrato, R. Perez-Tomas, M. Martinez, A. Grabulosa and P. Gamez, *Inorg. Chem.*, 2021, **60**, 7974–7990.
28 A. F. A. Peacock, A. Habtemariam, R. Fernandez, V. Walland, F. P. A. Fabbiani, S. Parsons, R. E. Aird, D. I. Jodrell and P. J. Sadler, *J. Am. Chem. Soc.*, 2006, **128**, 1739–1748.
29 S. Infante-Tadeo, V. Rodríguez-Fanjul, C. C. Vequi-Suplicy and A. M. Pizarro, *Inorg. Chem.*, 2022, **61**, 18970–18978.
30 M. T. Ashby, S. S. Alguindigue and M. A. Khan, *Organometallics*, 2000, **19**, 547–552.
31 R. Schuecker, R. O. John, M. A. Jakupec, V. B. Arion and B. K. Keppler, *Organometallics*, 2008, **27**, 6587–6595.
32 J. W. Faller, B. P. Patel, M. A. Albrizzio and M. Curtis, *Organometallics*, 1999, **18**, 3096–3104.
33 F. Chotard, R. Malacea-Kabbara, C. Balan, E. Bodio, M. Picquet, P. Richard, M. Ponce-Vargas, P. Fleurat-Lessard and P. Le Gendre, *Organometallics*, 2018, **37**, 812–820.
34 J. W. Faller and J. Parr, *Organometallics*, 2000, **19**, 3556–3561.
35 M. Hanif, A. A. Nazarov, C. G. Hartinger, W. Kandioller, M. A. Jakupec, V. B. Arion, P. J. Dyson and B. K. Keppler, *Dalton Trans.*, 2010, **39**, 7345–7352.
36 A. G. Bell, W. Kozminski, A. Linden and W. vonPhilipsborn, *Organometallics*, 1996, **15**, 3124–3135.
37 R. C. Sun, X. D. Chu, S. W. Zhang, T. Y. Li, Z. Wang and B. L. Zhu, *Eur. J. Inorg. Chem.*, 2017, 3174–3183.
38 X. T. Liu, X. Y. Han, Y. Wu, Y. Y. Sun, L. Gao, Z. Huang and Q. W. Zhang, *J. Am. Chem. Soc.*, 2021, **143**, 11309–11316.
39 E. Rutkowska, K. Pajak and K. Jozwiak, *Acta Pol. Pharm.*, 2013, **70**, 3–18.
40 W. L. F. Armarego, *Purification of Laboratory Chemicals*, Butterworth-Heinemann, Oxford, Eighth edn., 2017.
41 Y. Fu, A. Habtemariam, A. M. Pizarro, S. H. van Rijt, D. J. Healey, P. A. Cooper, S. D. Shnyder, G. J. Clarkson and P. J. Sadler, *J. Med. Chem.*, 2010, **53**, 8192–8196.
42 M. M. Vinogradov, Y. N. Kozlov, D. S. Nesterov, L. S. Shul'pina, A. J. L. Pombeiro and G. B. Shul'pin, *Catal. Sci. Technol.*, 2014, **4**, 3214–3226.
43 A. E. Fields, D. Zurwell, C. W. Padgett and B. Quillian, *J. Organomet. Chem.*, 2017, **846**, 66–73.
44 M. X. Cui, X. Y. Guo, H. H. Y. Sung, I. D. Williams, Z. Y. Lin and G. C. Jia, *Organometallics*, 2020, **39**, 2142–2151.
45 K. O. Biriukov, M. M. Vinogradov, O. I. Afanasyev, D. V. Vasilyev, A. A. Tsygankov, M. Godovikova, Y. V. Nelyubina, D. A. Loginov and D. Chusov, *Catal. Sci. Technol.*, 2021, **11**, 4922–4930.
46 J. Juanhuix, F. Gil-Ortiz, G. Cuni, C. Colldelram, J. Nicolas, J. Lidon, E. Boter, C. Ruget, S. Ferrer and J. Benach, *J. Synchrotron Radiat.*, 2014, **21**, 679–689.
47 G. M. Sheldrick, *SAINT and SADABS*, Bruker AXS Inc., Madison, Wisconsin, USA, 2012.
48 G. M. Sheldrick, *Acta Crystallogr., Sect. A: Found. Adv.*, 2015, **71**, 3–8.
49 G. M. Sheldrick, *Acta Crystallogr., Sect. C: Struct. Chem.*, 2015, **71**, 3–8.
50 O. V. Dolomanov, L. J. Bourhis, R. J. Gildea, J. A. K. Howard and H. Puschmann, *J. Appl. Crystallogr.*, 2009, **42**, 339–341.